nature physics

ARTICLES

https://doi.org/10.1038/s41567-018-0089-9

Geometric constraints during epithelial jamming

Lior Atia[1,8], Dapeng Bi[2,8], Yasha Sharma[1,8], Jennifer A. Mitchel[1], Bomi Gweon[1,3], Stephan A. Koehler[1], Stephen J. DeCamp[1], Bo Lan[1], Jae Hun Kim[1], Rebecca Hirsch[1], Adrian F. Pegoraro[4], Kyu Ha Lee[5], Jacqueline R. Starr[5], David A. Weitz[4], Adam C. Martin[6], Jin-Ah Park[1], James P. Butler[1,7] and Jeffrey J. Fredberg[1]*

As an injury heals, an embryo develops or a carcinoma spreads, epithelial cells systematically change their shape. In each of these processes cell shape is studied extensively whereas variability of shape from cell to cell is regarded most often as biological noise. But where do cell shape and its variability come from? Here we report that cell shape and shape variability are mutually constrained through a relationship that is purely geometrical. That relationship is shown to govern processes as diverse as maturation of the pseudostratified bronchial epithelial layer cultured from non-asthmatic or asthmatic donors, and formation of the ventral furrow in the *Drosophila* embryo. Across these and other epithelial systems, shape variability collapses to a family of distributions that is common to all. That distribution, in turn, is accounted for by a mechanistic theory of cell–cell interaction, showing that cell shape becomes progressively less elongated and less variable as the layer becomes progressively more jammed. These findings suggest a connection between jamming and geometry that spans living organisms and inert jammed systems, and thus transcends system details. Although molecular events are needed for any complete theory of cell shape and cell packing, observations point to the hypothesis that jamming behaviour at larger scales of organization sets overriding geometric constraints.

Grain in a silo, sand in a pile or beans in a chute can flow in some circumstances or become jammed in others[1–3]. Even bubbles comprising a foam or colloid particles comprising a suspension can jam or unjam. In each case, constituent particles interact with their nearest neighbours to form a disordered collective, and the collective as a whole can exhibit a transition from a fluid-like unjammed phase toward a solid-like jammed phase. A characteristic feature of the jamming phenomenon is that thermal fluctuations by themselves are insufficient to drive local structural rearrangements. The collective can therefore become trapped away from thermodynamic equilibrium and stuck in packing geometries that remain disordered in solid-like and fluid-like phases alike. Disordered geometry near the solid-like phase is thought to result from caging of each constituent particle by its immediate neighbours, force chains that percolate from particle to particle, and associated cooperative particle–particle interactions[1–3]. Within such collective systems, the jamming phenomenon is virtually ubiquitous.

To a surprising extent, similar phenomena typify the cellular collective comprising the confluent epithelial layer[4–10]. Constituent cells can migrate in multicellular packs and swirls reminiscent of fluid flow, with embryonic development, cancer invasion and wound healing being classical examples. Alternatively, they can become quiescent, solid-like and non-migratory, as in the mature, uninjured epithelium. Moreover, these solid-like versus fluid-like phases of the epithelial collective have been linked to cell caging by immediate neighbours, propagating force chains and cooperative cell–cell interactions that typify cell jamming and unjamming[4–10]. However, every analogy has its limits and, compared to that within the inert granular collective, the cellular packing geometry that defines a confluent epithelial collective would seem to be quite a different matter controlled by altogether different mechanisms[9,11–14].

Detailed measurements of epithelial packing geometry and associated cell-to-cell shape variability described below lead to two striking findings. Here we report, first, that measurements spanning diverse confluent epithelial systems scale to a statistical shape distribution that is virtually common to all. As a result, cell shape and shape variability are mutually constrained through a relationship that is purely geometrical. We show, second, that these shape distributions are reminiscent of the Edwards conjecture, which holds that among the immense number of packing geometries that is possible within a jammed granular collective, all are equally likely[15,16]. However, how the physics of granular matter can be adapted in a more satisfying way to the biology of the space-filling, highly adaptable, active particles that comprise a confluent epithelial collective remains an open question (Supplementary Section 1). Nevertheless, the findings described here deepen the analogy between the physics of the inert granular collective and that of the living epithelial collective, making this analogy all the more striking, and all the more curious[4–10].

Shape and shape variability in vitro

Human bronchial epithelial cells (HBECs) were grown to confluence in submerged conditions on a porous Transwell insert for 5–6 days and then allowed to mature in air–liquid interface culture conditions to become well differentiated over the course of 6–20 days. Migratory dynamics were used to confirm evidence of progressive cell jamming[4] (Supplementary Section 2 and Supplementary Fig. 1), and a variety of imaging modalities were used to quantify cellular morphology (Methods and Supplementary Sections 3 and 4).

[1]Harvard T.H. Chan School of Public Health, Boston, MA, USA. [2]Department of Physics, Northeastern University, Boston, MA, USA. [3]Department of Biomedical Engineering, Hanyang University, Seoul, Korea. [4]Harvard University, School of Engineering and Applied Sciences, Cambridge, MA, USA. [5]The Forsyth Institute, Cambridge, MA, USA. [6]Department of Biology, Massachusetts Institute of Technology, Cambridge, MA, USA. [7]Department of Medicine, Brigham and Women's Hospital and Harvard Medical School, Boston, MA, USA. [8]These authors contributed equally: Lior Atia, Dapeng Bi, Yasha Sharma. *e-mail: jfredber@hsph.harvard.edu

In HBEC layers from both non-asthmatic and asthmatic donors, areas and aspect ratios (ARs; Methods) were highly variable (Fig. 1a,b). Consistent with previous reports[4], cells from asthmatic donors were more elongated than their non-asthmatic counterparts, and the distributions of ARs were broad and skewed (Fig. 1c and Supplementary Fig. 2). As a simple measure of shape variability from cell to cell, we used the standard deviation of the aspect ratio, s.d.(AR). We had thought of this shape variability as representing biological noise. We were therefore surprised to find that data from all non-asthmatic donors and all days of maturation traced an unanticipated but clear linear relationship between the mean of the aspect ratio, $\overline{\mathrm{AR}}$, and s.d.(AR) ($P<0.0005$; Fig. 1d and Supplementary Table 1). Specifically, as the cell aspect ratio became progressively smaller with increasing days of maturation, its variability from cell to cell did so as well (Fig. 1d, top left inset). Cells from asthmatic donors mature more slowly and migrate more quickly than those from non-asthmatic donors[4]. We had therefore expected that any relationship between cell shape and its variability would be different as well between non-asthmatic versus asthmatic donors. To our further surprise, $\overline{\mathrm{AR}}$ and s.d.(AR) from all asthmatic donors and all days of maturation defined a closely similar linear relationship, although with a slightly smaller slope ($P<0.0005$; Fig. 1d and Supplementary Table 1). Moreover, when we pooled all cells from all fields of view, and for each day of maturation, $\overline{\mathrm{AR}}$ and s.d.(AR) for both asthmatic and non-asthmatic donors traced virtually the same relationship (Fig. 1d , top left inset). However, within this relationship, mature and/or non-asthmatic cells tended to have lower values of $\overline{\mathrm{AR}}$ and s.d.(AR) whereas immature and/or asthmatic cells tended to have larger values (Fig. 1d, top left inset, and Supplementary Fig. 2d).

Shape and shape variability in vivo

We then considered that this geometric relationship might reflect a peculiarity of HBECs, an idiosyncrasy of layer maturation or an artefact of cell culture. We show that the geometric relationship traced by the data in Fig. 1d and Supplementary Movie 1 is not limited to HBECs, and is not a specific effect of the passage of time, layer maturation or cell crowding; these factors all mattered but no one among them could fully explain the observations (Fig. 1d, bottom right inset; Supplementary Section 5). To rule out artefacts of cell culture and, more importantly, to test the relationship between shape and shape variability in a completely distinct epithelial system in vivo, we studied ventral furrow formation in the developing embryo of the fruit fly *Drosophila melanogaster*[11].

In *Drosophila* development, the ventral furrow forms to bring mesodermal precursor cells into the interior of the embryo. In this process, cells exhibit pulsatile contractions that transition from a relaxed to a sustained contractile state[17,18]. These events are accompanied by changes in cell shape that include apical flattening, constriction of apical diameter, cell elongation and subsequent shortening (Fig. 2a,b, left column)[19]. Across multiple wild-type embryos, we characterized the AR of cell apical domains and its variability as cells constricted, increased their movement within the epithelial plane (towards the ventral midline in the wild type) and escaped their arrested state (Fig. 2c left column), but before the cells invaginated (Methods). Even though the *Drosophila* embryonic epithelium differs in many regards from HBEC and Madin–Darby canine kidney (MDCK) cell layers in vitro, cell shape data obtained in this system as the furrow forms traced the same geometric relationship (Fig. 2d, left and Supplementary Movie 2). To test how shape and shape variability are affected by genetic variability, we studied embryos that were mutant for concertina (*cta*). The *cta* gene encodes a $G\alpha_{12/13}$ protein, which is required for coordinated apical constriction[20]. In *cta* maternal-effect mutants, cells of the ventral furrow constrict in an uncoordinated manner and furrow formation becomes slow and uneven[21]. We also used RNA-mediated interference (RNAi) to knock down the transcription factor Twist, which is essential for sustained apical contraction and ventral furrow formation. Unlike in the maturing HBEC layer, but similar to compression-induced unjamming of the HBEC layer, these events in the embryo were accompanied by progressive increases of cellular speeds and $\overline{\mathrm{AR}}$ values in tandem (Fig. 2c, centre and right), and tracked with time from smaller toward larger $\overline{\mathrm{AR}}$ and s.d(AR) (Fig. 2d centre and right, and Supplementary Movies 3 and 4). Moreover, gradual transitions of layer structure (as reflected by changes in $\overline{\mathrm{AR}}$) and cooperative dynamics (as reflected by changes in the self-overlap order parameter and the four-point susceptibility), occurred simultaneously (Supplementary Fig. 1). These data suggest that certain changes in cell morphology during ventral furrow formation are associated with epithelial layer unjamming. However, it remains unclear whether unjamming and the associated solid-like to fluid-like transition in that particular context are permissive of the cellular flows that are driven by apical actomyosin constriction, or are the effect[17].

Diverse systems reveal common shape distributions

We found that explanations based solely on the mathematics of randomness and tessellation are at best incomplete (Supplementary Fig. 3). To explain these findings at a deeper level, we reasoned that the underlying statistical distributions of observed cell shapes across these diverse epithelial systems must comprise a special subclass of distributions that has yet to be determined. To fill that gap, we measured for each of the biological cases above the corresponding probability density functions (PDFs) of observed ARs, as described below. We then went on to ask what physical mechanism might account for that special subclass and its statistical properties.

During maturation of HBECs or MDCKs, cell shapes became systematically less elongated and less variable with time (Fig. 3a,c). In contrast, during the approach to the formation of the ventral furrow in the wild-type *Drosophila* embryo, the cell shapes became more elongated and more variable with time (Fig. 3e). In the *cta* mutant compared with the wild type, the cell shape was more elongated and more variable, and even more so in the Twist knockdown (Fig. 3e). Despite differences in PDFs within and between these systems, and regardless of their trajectories over time, the functional forms of all respective PDFs were unimodal and skewed in a manner suggestive of a common underlying mathematical basis (Fig. 3a,c,e). To assess this commonality in a quantitative fashion, we rescaled AR to the form $x=(\mathrm{AR}-1)/(\overline{\mathrm{AR}}-1)$; importantly, the $\overline{\mathrm{AR}}$ in HBECs progressively decreased with increasing days of maturation ($P<0.0005$; Supplementary Fig. 1), and was systematically greater in non-asthmatic versus asthmatic cells ($P<0.0005$). Rescaling in this fashion maps the lower limits of the abscissa and the ordinate to zero, and scales the mean of the distribution to unity. Across all days of maturation for HBEC data in all non-asthmatic donors, data thereupon collapsed onto a common distribution (Fig. 3a,b). For asthmatic donors, too, rescaled data again collapsed to a common distribution (Fig. 3a,b), as did data from MDCK cells (Fig. 3c,d), events preceding formation of the ventral furrow, and interventions that disrupt that furrow formation (Fig. 3e,f).

Generic connections between jamming and geometry

Remarkably, within and across these diverse epithelial layers, observed variability of shape from cell to cell was well described by a single distribution that, with small distinctions, was common to all. Importantly, a direct consequence of distributions that are invariant to scaling in this manner is a linear relationship between $\overline{\mathrm{AR}}$ and s.d.(AR), as seen in Figs. 1 and 2.

We wondered, therefore, whether the findings above might be explained by a generic empirical connection between jamming and geometry that is not restricted to the particular effects of cell maturation, cortical tension or cell–cell adhesion, and instead points to a larger jamming reference class that transcends such system details

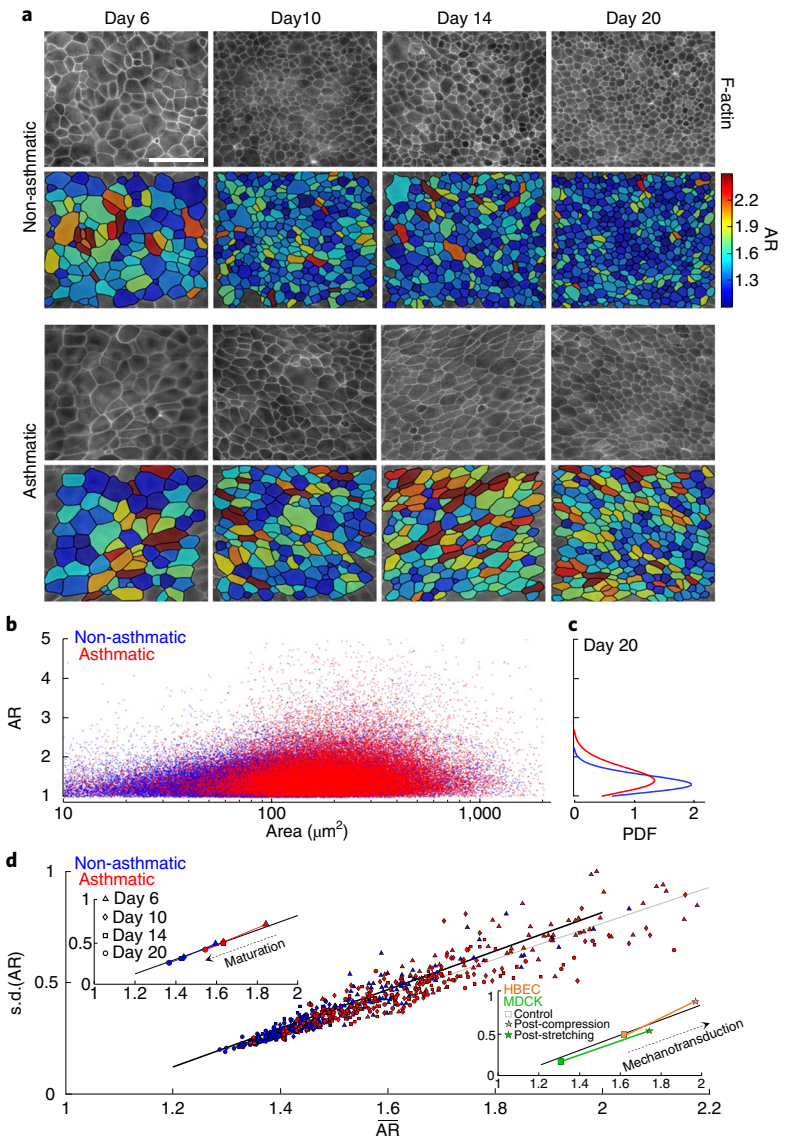

Fig. 1 | Across non-asthmatic and asthmatic donors of primary HBECs, and across all days of maturation, cell shape and shape variability in vitro are mutually constrained. a, The apical actin ring was used to measure projected cell area and cell AR (Methods and Supplementary Figs. 9–11). With ongoing layer maturation, the AR of both non-asthmatic and asthmatic cells became progressively smaller and less variable (corresponding colour maps). Scale bar, 50 μm. **b**, In cells from both non-asthmatic donors ($n = 87{,}066$ cells, blue) and asthmatic donors ($n = 46{,}076$ cells, red), AR was highly variable but did not co-vary with projected cell area. **c**, In the mature layer (20 days), the distributions of AR in both non-asthmatic and asthmatic cells were wide and skewed. **d**, AR from all donors and all days of maturation defined a clear relationship between the mean of AR ($\overline{AR}$) and the standard deviation (s.d.) of AR (each datum represents a different field of view), with non-asthmatic cells (days 6, 10, 14 and 20; respectively, $n = 13{,}293$, 23,624, 20,371 and 29,778) tending to have lower values of $\overline{AR}$ and s.d.(AR), and asthmatic cells (days 6, 10, 14 and 20; respectively, $n = 5{,}372$, 12,629, 10,019 and 18,056) tending to have larger values. Top left inset, with increasing days of maturation, $\overline{AR}$ and s.d.(AR) decreased in tandem (each datum pools all cells for a given day of maturation), but were systematically increased in asthmatic compared with non-asthmatic controls. Nevertheless, all observations fell onto the same relationship. Bottom right inset, to rule out the possibility that this relationship might reflect an idiosyncrasy of layer maturation, we studied changes in cell shape and shape variability that occur acutely in response to an imposed mechanical perturbation. As demonstrated previously, for example, application of an apical-to-basal pressure difference (30 cm H_2O) across the porous Transwell insert causes the mature, jammed, HBEC layer to unjam[4,36,37] (Supplementary Section 2). Whereas maturation caused changes in cell shape to track in time from larger to smaller $\overline{AR}$ and s.d.(AR), indicative of progressive jamming, mechanical compression caused changes in cell shape to track in the opposite direction with time, from smaller to larger $\overline{AR}$ and s.d.(AR) (control, $n = 6{,}153$; post-compression, $n = 5{,}659$), indicative of unjamming. Comparing unjamming and jamming, these changes with time were opposite in sign but tracked up or down a geometric relationship that in both instances was the same (bottom right and top left insets in **d**). To complement results from HBEC compression, we applied sequential stretches to the mature MDCK layer plated on a deformable substrate (6% strain amplitude, isotropic in the cell plane, 1 s duration, once every 6 s for 20 min). Immediately after stretch cessation, cell shapes became elongated, but within 60 min these changes relaxed back to pre-stretch values (control, $n = 367$; post-compression, $n = 422$). These acute changes in cell shape could not be accounted for by changes in cell crowding, which were small (Supplementary Fig. 2d for HBECs). As such, the geometric relationship traced by the data (**d**) is not a specific effect of the passage of time, layer maturation or cell crowding; these factors all mattered but no one among them could account for the observed geometric relationship. The dark continuous lines in **d** are not regression lines, but rather the prediction given by the computational model of cell–cell interactions (Supplementary Section 6 and Supplementary Fig. 12). The light continuous line in **d** represents a linear regression for all data that gives s.d.(AR) $= 0.808\overline{AR} - 0.85$ ($R^2 = 0.878$).

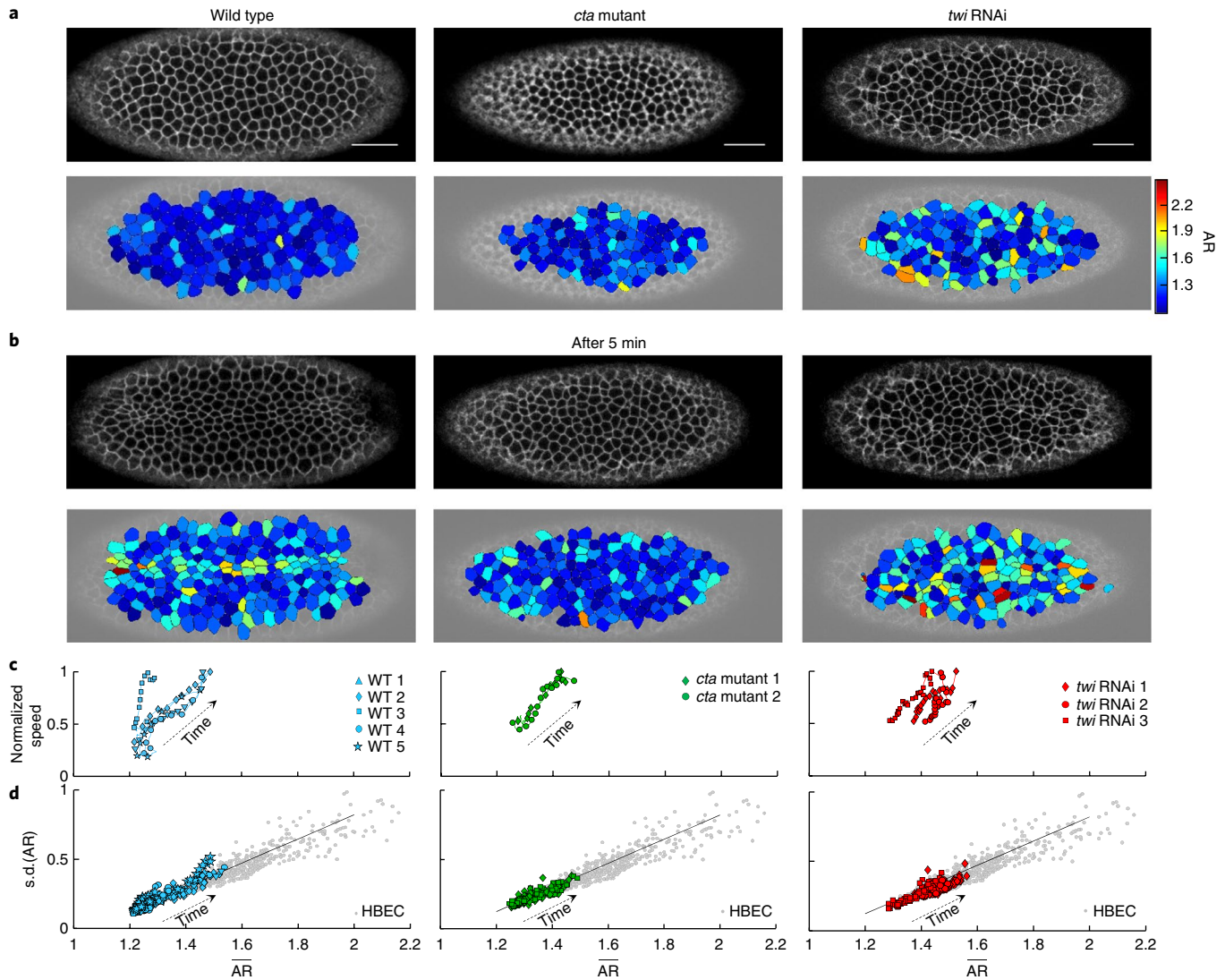

Fig. 2 | During ventral furrow formation in *Drosophila* in vivo, cell shape and shape variability follow the same geometric relationship as HBECs in vitro. **a**,**b**, During *Drosophila* ventral furrow formation, a membrane marker was used to identify cell–cell boundaries in wild-type (WT), concertina (*cta*) mutant and Twist (*twi*) RNAi embryos ($n=5$, 2 and 3, respectively). The AR was measured for 100–150 cells per frame, for 60–100 frames (6–8 seconds apart) per embryo. With time (**b**, after 5 min), cells constricted and attempted to form the ventral furrow, and the cell AR in all embryos became progressively larger and more variable (corresponding colour maps). Scale bars, 25 μm. **c**, The average speed in the epithelial plane (across all cells) and AR increased in tandem for wild-type, *cta* mutant and *twi* RNAi embryos. The speed is normalized to the maximum speed observed in each embryo, typically corresponding with the initiation of the fold, and ranging from 3 μm min^{-1} in wild-type to 1.5 μm min^{-1} in *cta* mutant and *twi* RNAi embryos. **d**, With time, AR and s.d.(AR) increased in tandem in wild-type embryos (left) and followed the same geometric relationship as seen in HBECs in vitro (Fig. 1d and Supplementary Movies 2–4). This relationship persisted in embryos with genetic variability (centre and right) that prevents or hinders the ventral furrow formation, as in *cta* mutant and *twi* RNAi embryos, respectively. (Each datum represents a frame from an individual embryo.) Each grey datum represents a different field of view for both asthmatic and non-asthmatic HBECs. The dark continuous line is the same as in Fig. 1, and corresponds to the prediction given by the computational model (Supplementary Section 6 and Supplementary Fig. 12).

(Fig. 4 and Supplementary Fig. 4). As a guide for thought, we start by considering the well-studied case of the disordered granular collective; recent evidence points to fluid–solid transitions in disordered granular matter as being similar in two and three dimensions[22,23]. In three dimensions, grain centres can be used to tessellate the volume around each individual grain. When packing is dense and disordered, these tessellated volumes necessarily vary from grain to grain. In such a physical system, the distribution of volumes, x, has been found theoretically and confirmed empirically to follow the k-gamma distribution[24],

$$\mathrm{PDF}(x;k) = k^k x^{k-1} \mathrm{e}^{-kx} / \Gamma(k) \qquad (1)$$

where $\Gamma(k)$ is the Legendre gamma function. This distribution is fully described by only a single parameter, k, and has a mean of unity.

Equation (1) arises from statistical mechanics based in part on volume exclusion, which prevents two grains from occupying the same space at the same time, and tessellated volume fluctuations that are additive so as to account for total system volume. We note that the derivation of this result[24] does not depend on the dimensionality of the system, and therefore applies as well to granular systems in two and three dimensions alike. In a confluent cellular system, however, cellular aspect ratios are in no sense additive, and for that reason and others there currently exists no rigorous basis for the applicability of the k-gamma distribution to metrics of cell shape.

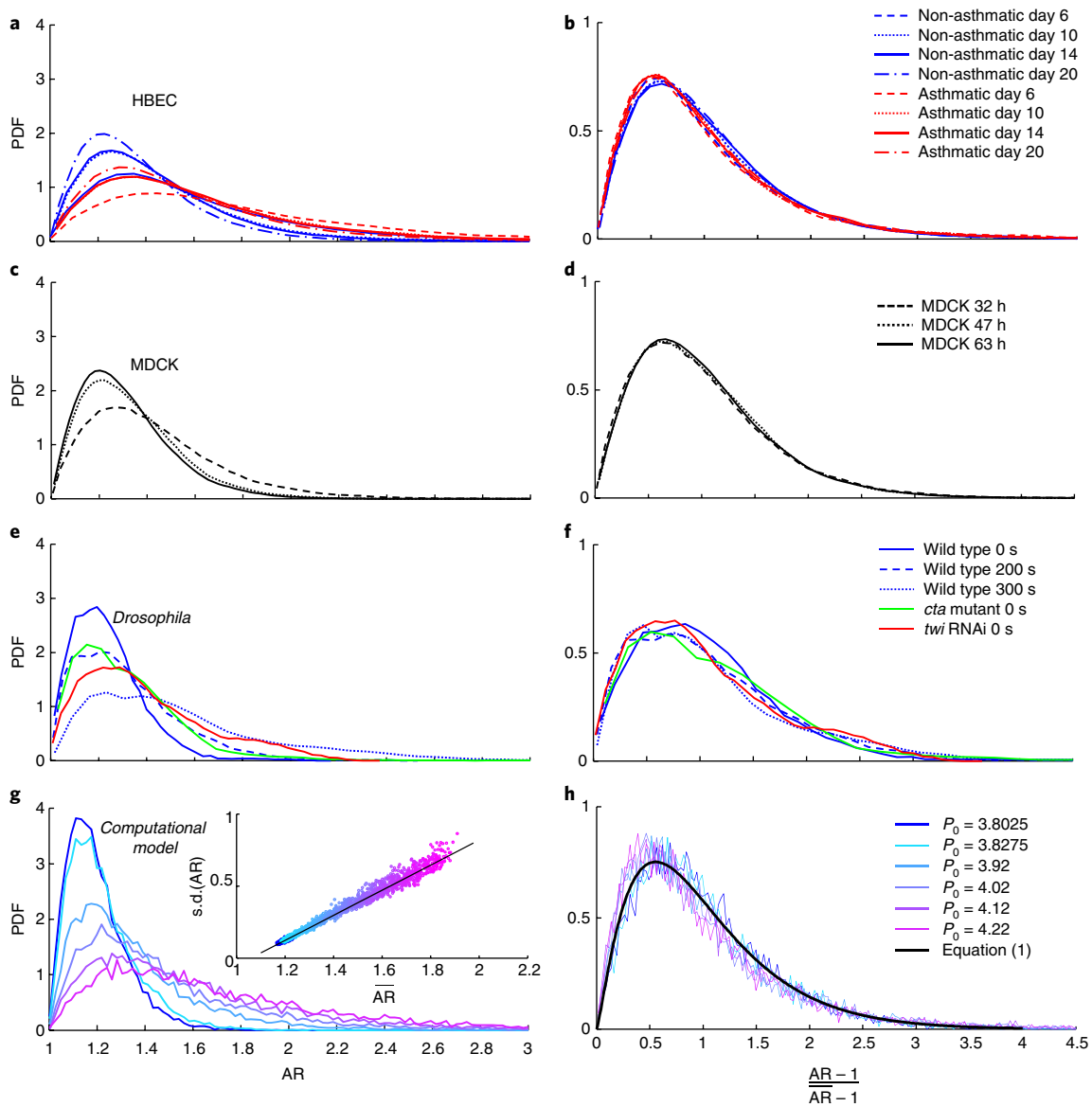

Fig. 3 | Within and across vastly different epithelial systems, shape variability collapses to a family of PDFs that is common to all, and perhaps universal. a, PDFs of AR in HBECs (Fig. 1d, main panel and top left inset) became systematically less skewed and less variable with maturation. **b**, PDFs of the rescaled parameter $x=(\mathrm{AR}-1)/(\overline{\mathrm{AR}}-1)$ of HBECs, where $\overline{\mathrm{AR}}$ denotes the mean AR for each respective distribution, followed a k-gamma distribution (equation (1)) with $k=1.97$. **c**,**d**, Similar to **a**,**b**, respectively, for MDCKs with $k=2.31$. **e**,**f**, Similar to **a**,**b**, respectively, for *Drosophila* (Fig. 2d) with $k=2.52$. **g**, Predicted distributions for AR given by the model in refs [26,27]. For increasing values of the model's input parameter P_0, the inset shows the predicted relationship for $\overline{\mathrm{AR}}$ versus s.d.(AR) (Supplementary Section 6 and Supplementary Fig. 12). **h**, Collapse of predicted distributions. The black line shows the maximum-likelihood-estimation fit with $k=2.53$.

Nevertheless, when a layer remains confluent, each individual cell can change not only its area but also its shape at the expense of complementary changes in neighbouring cells. A central role for cell shape is demonstrated, for example, in the case of unjamming caused by acute layer compression, which—compared with the case of layer maturation—reveals changes of area per cell and area distributions that are small but changes of cell shape and shape distributions that are not small (Fig. 1d inset and Supplementary Fig. 2d).

For these reasons and others, the statistical physics of cell jamming emphasizes cell shape and its changes[4,5,9,25–29]. Statistical physics of cell jamming also leads to a prediction for the distribution of energy barrier heights that act to impede local cellular rearrangements, where the k-gamma distribution is seen to arise yet again[26]. These hints lead us to the conjecture that cell shapes, too, are governed by a k-gamma distribution. We cannot prove this conjecture analytically, but using the extensive data sets described above we can test it empirically. Specifically, we take $x=(\mathrm{AR}-1)/(\overline{\mathrm{AR}}-1)$ and use maximum-likelihood estimation (Methods). Equation (1) is then seen to be faithful to observations with a high degree of statistical confidence (Supplementary Figs. 5 and 6). In HBECs, the parameter k varied little over all days of maturation ($P<0.0005$, Supplementary Fig. 5b) and, moreover, did not differ between non-asthmatic versus asthmatic cells ($P=0.2147$, Supplementary Fig. 5b). Much as in the case of jammed granular packings[24], but quite unlike the case of unjammed granular packings, k changed only slightly as the system became progressively more jammed (Supplementary Fig. 5b; see also Supplementary Section 6; compare Fig. 4 in ref. [24]). Even though some differences in k were statistically significant, these differences were at most modest and, to a reasonable approximation, k in HBECs could be taken as a constant value

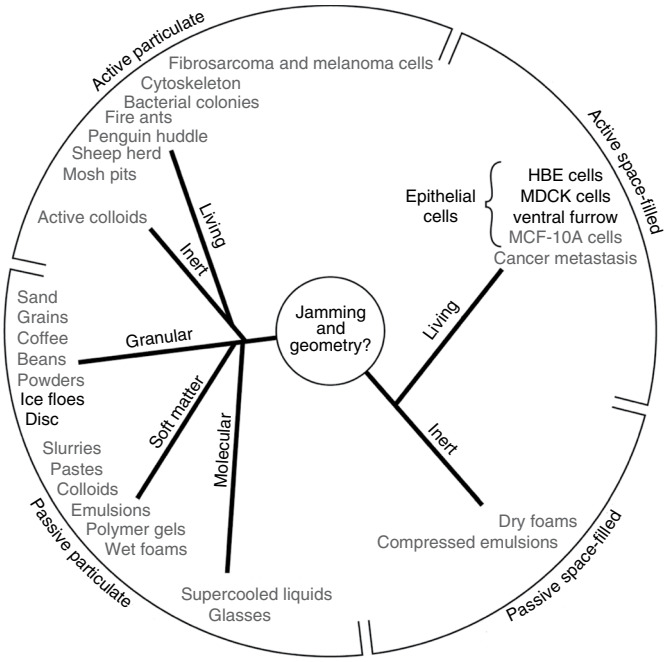

Fig. 4 | The jamming superfamily. Each entry denotes a physical system in which jamming behaviour has been reported, and is categorized here into one of four jamming classes. The systems described in this report are shown in bold (see also Supplementary Fig. 4). The jamming mechanism was first introduced to explain the poorly understood behaviours that typify certain collective granular systems. However, similarities in behaviour between such inert granular systems and the migrating epithelial layer were quickly recognized[6,38,39]. For example, both granular and cellular collective systems are close-packed, volume exclusion prevents two particles (or cells) from occupying the same space at the same time, and particle–particle (cell–cell) interactions are strong. Moreover, just as inert granular systems display swirling motions that arise in cooperative multi-particle packs and clusters, so too does the migrating epithelial layer[8,40–44]. However, other physical factors do not fit so easily into this analogy. For example, within granular matter the state of internal mechanical stress is mainly compressive—these are fragile materials in the sense that they can support immense compressive stresses but can support no tensile stress whatsoever—whereas within the confluent cell layer the mechanical stress is overwhelming tensile[42]. Within granular matter, a principal control variable for jamming is free space between grains[2,45], whereas in the fully confluent cell layer there is by definition no free space between cells. Within granular matter neither a change of particle shape nor mutual particle–particle adhesion is required for jamming or unjamming—although either can influence jamming dynamics[46]—whereas cell shape change and cell–cell adhesion are thought to be indispensable features of epithelial function and jamming[5,25–27]. Perhaps most importantly, the granular particle is neither active nor self-propulsive nor mechanosensitive, whereas the epithelial cell exhibits all of these characteristics. In this report, we show that the behaviour of these diverse living and inert systems is unified to a remarkable extent by consideration of system geometry.

of 1.97 (95% confidence interval (CI) [1.89, 2.04]). In MDCK cells, we found, similarly, that all data were well represented by a single k value of 2.31 (CI [1.90, 2.73]). In *Drosophila*, k values were not statistically different between the wild type and *cta* mutant ($P=0.023$), or Twist RNAi ($P=0.762$) (Supplementary Fig. 6b), and were well represented by a single k value of 2.52 (CI [2.43, 2.62]). Across these diverse epithelial systems, equation (1) pertained throughout and k was bounded to the relatively narrow range between 2 and 2.5. The near-universal structure of shape distributions, and with a virtually common value of k, is therefore all the more striking.

Effective temperature in jammed packings

For disordered granular matter, the mathematical form of the k-gamma distribution (equation (1)) constrains volume variability to mean volume according to the relationship s.d. $(V)=(\overline{V}-V_{\min})/\sqrt{k}$, where V represents the local tessellated volume associated with each individual grain, $\overline{V}$ is the mean value of such volumes and $V_{\min}$ is the minimal random packing volume that the system can attain[24]. However, just as equation (1) requires the volume variability s.d.(V) to change linearly with the mean volume $\overline{V}$ in the case of granular systems, so too equation (1) requires the cell shape variability s.d.(AR) to change linearly with the mean cell shape $\overline{\mathrm{AR}}$ in the case of epithelial systems (Figs. 1d and 2d). But is there a deeper insight that might help to explain these empirical findings?

Of the great many possible jammed packings into which a collective granular system might become trapped, all jammed packings become equally likely just as the system approaches the transition between fluid-like and solid-like phases; this is called the Edwards conjecture, and has recently been proved[15,16]. If no one jammed configuration is privileged over another, then the distributional entropy, S, becomes maximized, from which it has been shown that equation (1) follows directly[24]. In a jammed packing, however, thermal fluctuations are insufficient to drive local rearrangements, and for that reason the traditional statistical mechanics of Gibbs do not apply. Nevertheless, if volume in an athermal granular system were to play a role analogous to that of energy in a thermodynamic system, as suggested by Edwards, one can then define an effective temperature, T_{eff}, given by $1/(\partial S/\partial V)$[15,24]. Carried over from volume variability in granular jamming to shape variability in cellular jamming, T_{eff} then takes the form

$$T_{\mathrm{eff}}=\mathrm{s.d.(AR)}/\sqrt{k}=(\overline{\mathrm{AR}}-\mathrm{AR}_{\min})/k \qquad (2)$$

To the extent that equation (1) pertains (Fig. 3b,d,f) and to the extent that observed changes in k across diverse epithelial systems are small (Supplementary Figs. 5b and 6b), then the cell jamming mechanism and equation (2) would explain not only the existence of a relationship between cell shape variability and cell shape, but

also its linearity and its invariance. Through the lens of such a physical picture, data in the lower left of Fig. 1d might then be imagined as corresponding to effectively 'cooler' states, and those at the upper right to relatively 'warmer' states. It remains to be determined, however, whether effectively warmer, unjammed, migratory, fluid-like phases are harnessed to enable wound healing, development or invasion, and effectively cooler, jammed, non-migratory, solid-like phases are harnessed to slow those processes or arrest them.

Experimental observations of cell shape spanning diverse epithelia, the statistical physics of disordered granular matter and computational mechanics of cell–cell interactions (Supplementary Section 6) are thus seen to converge in a manner that is qualitatively consistent and quantitatively reinforcing.

Geometric constraints on cell shape variation

As early as 36 BC, the Roman Marcus Terentius Varro suggested that the bee's honeycomb, in order to enclose a cellular space, makes optimal use of material. It was only much later, in 1611, when Johannes Kepler proposed that hexagonal packing of identical spheres corresponds to the densest possible arrangement. D'Arcy Thompson later argued that biological systems evolve toward and thus tend to recapitulate such optimal packing structures[30]. These conjectures and others dating even earlier have been proved only recently[31,32]. Cell divisions and apoptosis are known to drive cell arrangements away from such a hexagonal packing, however, and toward an equilibrium distribution of polydisperse cellular polygons[12]. Nevertheless, shape distributions measured throughout the jamming process of HBECs depart systematically from that predicted equilibrium distribution (Supplementary Fig. 2e).

A variety of dynamic events were probably at work in the data sets reported here, including but not limited to proliferation, crowding, extrusion, apoptosis and even newly discovered nematic defects[14], any of which might be expected to impact the jamming state of the epithelial collective. Nevertheless, in instances when $\overline{\text{AR}}$ and s.d.(AR) are relatively small, the configurational options from which the cellular collective can sample are correspondingly limited, cell movements become highly constrained, rearrangements among neighbouring cells become slowed and the collective as a whole becomes solid-like. This is the essence of the jammed state. By contrast, in instances when $\overline{\text{AR}}$ and s.d.(AR) are relatively large, a wider range of configurational options become available, cell movements become less constrained, rearrangements among neighbouring cells become increasingly frequent and the collective as a whole becomes fluid-like (Supplementary Movies 1–4). This is the essence of the unjammed state.

The fundamental open questions are these. First, experimental results establish that scaled ARs are distributed in a fashion that is approximately common to all and follow the k-gamma distribution, which in turn requires a linear relationship between $\overline{\text{AR}}$ and s.d.(AR). However, why this should be true, and why the numerical value of k in those systems should be so narrowly limited remain unexplained. Second, does structural disorder within a multicellular tissue represent noise (that is, an inconsequential by-product of more consequential biological events)? Alternatively, might disorder be physiologically useful in its own right? New experimental evidence presented here and elsewhere increasingly ties cell jamming together with structural disorder, cell mechanics and collective migration[4–10]. However, the extent to which graded degrees of cell jamming and disorder might be regulated physiologically, or dysregulated pathologically, remains unclear. Importantly, both cell jamming and contact inhibition of locomotion have argued to account for the progressive slowdown of cellular motions within the confluent epithelial layer[33]. However, it remains unclear whether these mechanisms are distinct, and, if so, the extent to which they are mutually independent, interdependent or reinforcing. Finally, the biology of metastatic disease currently lacks a mechanistic explanation for how collective cancer cell migration can occur when the epithelial-to-mesenchymal transition program is inactive[34,35]. The extent to which the unjamming transition comprises an alternative gateway to cancer cell migration and metastasis remains to be established (Supplementary Section 1).

Data obtained across vastly different epithelial systems emphasize the generality of the cell jamming concept. Although molecular events are needed for any complete theory of cell shape and cell packing—whether during embryogenesis, cancer invasion, or wound healing—jamming behaviour at a larger scale of organization is seen to set overriding geometric constraints. It is well recognized that molecular events cannot exert their effects on cell shape directly, but rather mediate their effects through the combined but indirect actions of genetic, cellular and mechanical inputs that remain incompletely understood[11]. Here we build directly on this idea and extend it from the singe cell to the epithelial collective. To set the most primitive features of cell shape and shape variability, these indirect actions combine to modulate the proximity of the confluent cell layer to the jammed state, and thereby shift the layer up or down the geometric relationship shown in Figs. 1–3. On the scale of cellular dimensions, therefore, these findings point to the hypothesis that cell jamming may be the principal determinant of epithelial cell shape and shape variability.

Methods

Methods, including statements of data availability and any associated accession codes and references, are available at https://doi.org/10.1038/s41567-018-0089-9.

Received: 2 November 2017; Accepted: 16 February 2018;
Published online: 02 April 2018

References

1. Liu, A. J. & Nagel, S. R. Jamming is not just cool any more. *Nature* **396**, 21–22 (1998).
2. Trappe, V., Prasad, V., Cipelletti, L., Segre, P. N. & Weitz, D. A. Jamming phase diagram for attractive particles. *Nature* **411**, 772–775 (2001).
3. de Gennes, P. & Badoz, J. *Fragile Objects: Soft Matter, Hard Science, and the Thrill of Discovery* (Copernicus, New York, NY, 1996).
4. Park, J. A. et al. Unjamming and cell shape in the asthmatic airway epithelium. *Nat. Mater.* **14**, 1040–1048 (2015).
5. Farhadifar, R., Roper, J. C., Aigouy, B., Eaton, S. & Julicher, F. The influence of cell mechanics, cell–cell interactions, and proliferation on epithelial packing. *Curr. Biol.* **17**, 2095–2104 (2007).
6. Sadati, M., Taheri Qazvini, N., Krishnan, R., Park, C. Y. & Fredberg, J. J. Collective migration and cell jamming. *Differentiation* **86**, 121–125 (2013).
7. Pawlizak, S. et al. Testing the differential adhesion hypothesis across the epithelial–mesenchymal transition. *New J. Phys.* **17**, 083049 (2015).
8. Nnetu, K. D., Knorr, M., Pawlizak, S., Fuhs, T. & Kas, J. A. Slow and anomalous dynamics of an MCF-10A epithelial cell monolayer. *Soft Matter* **9**, 9335–9341 (2013).
9. Kim, S. & Hilgenfeldt, S. Cell shapes and patterns as quantitative indicators of tissue stress in the plant epidermis. *Soft Matter* **11**, 7270–7275 (2015).
10. Garcia, S. et al. Physics of active jamming during collective cellular motion in a monolayer. *Proc. Natl Acad. Sci. USA* **112**, 15314–15319 (2015).
11. Gilmour, D., Rembold, M. & Leptin, M. From morphogen to morphogenesis and back. *Nature* **541**, 311–320 (2017).
12. Gibson, M. C., Patel, A. B., Nagpal, R. & Perrimon, N. The emergence of geometric order in proliferating metazoan epithelia. *Nature* **442**, 1038–1041 (2006).
13. Xiong, F. et al. Interplay of cell shape and division orientation promotes robust morphogenesis of developing epithelia. *Cell* **159**, 415–427 (2014).
14. Saw, T. B. et al. Topological defects in epithelia govern cell death and extrusion. *Nature* **544**, 212–216 (2017).
15. Edwards, S. F. & Oakeshott, R. B. S. Theory of powders. *Physica A* **157**, 1080–1090 (1989).
16. Martiniani, S., Schrenk, K. J., Ramola, K., Chakraborty, B. & Frenkel, D. Numerical test of the Edwards conjecture shows that all packings are equally probable at jamming. *Nat. Phys.* **13**, 848–851 (2017).
17. Martin, A. C., Kaschube, M. & Wieschaus, E. F. Pulsed contractions of an actin-myosin network drive apical constriction. *Nature* **457**, 495–499 (2009).

18. Xie, S. & Martin, A. C. Intracellular signalling and intercellular coupling coordinate heterogeneous contractile events to facilitate tissue folding. *Nat. Commun.* **6**, 7161 (2015).
19. Sweeton, D., Parks, S., Costa, M. & Wieschaus, E. Gastrulation in *Drosophila*: the formation of the ventral furrow and posterior midgut invaginations. *Development* **112**, 775–789 (1991).
20. Parks, S. & Wieschaus, E. The *Drosophila* gastrulation gene concertina encodes a G alpha-like protein. *Cell* **64**, 447–458 (1991).
21. Xie, S., Mason, F. M. & Martin, A. C. Loss of Galpha12/13 exacerbates apical area dependence of actomyosin contractility. *Mol. Biol. Cell* **27**, 3526–3536 (2016).
22. Vivek, S., Kelleher, C. P., Chaikin, P. M. & Weeks, E. R. Long-wavelength fluctuations and the glass transition in two dimensions and three dimensions. *Proc. Natl Acad. Sci. USA* **114**, 1850–1855 (2017).
23. Illing, B. et al. Mermin–Wagner fluctuations in 2D amorphous solids. *Proc. Natl Acad. Sci. USA* **114**, 1856–1861 (2017).
24. Aste, T. & Di Matteo, T. Emergence of Gamma distributions in granular materials and packing models. *Phys. Rev. E* **77**, 021309 (2008).
25. Bi, D. P., Lopez, J. H., Schwarz, J. M. & Manning, M. L. Energy barriers and cell migration in densely packed tissues. *Soft Matter* **10**, 1885–1890 (2014).
26. Bi, D., Lopez, J. H., Schwarz, J. M. & Manning, M. L. A density-independent rigidity transition in biological tissues. *Nat. Phys.* **11**, 1074–1079 (2015).
27. Bi, D., Yang, X., Marchetti, M. C. & Manning, M. L. Motility-driven glass and jamming transitions in biological tissues. *Phys. Rev. X* **6**, 021011 (2016).
28. Sussman, D. M., Paoluzzi, M., Marchetti, M. C. & Manning, M. L. Anomalous glassy dynamics in simple models of dense biological tissue. Preprint at https://arxiv.org/abs/1712.05758 (2017).
29. Wilk, G., Iwasa, M., Fuller, P. E., Kandere-Grzybowska, K. & Grzybowski, B. A. Universal area distributions in the monolayers of confluent mammalian cells. *Phys. Rev. Lett.* **112**, 138104 (2014).
30. Thompson, D. A. W. *On Growth and Form* 88–125 (Cambridge Univ. Press, Cambridge, 1917).
31. Hales, T. et al. A formal proof of the Kepler conjecture. *Forum Math. Pi* **5**, 1–29 (2017).
32. Hales, C. T. The honeycomb conjecture. *Discret. Comput. Geom.* **25**, 1–22 (2001).
33. Puliafito, A. et al. Collective and single cell behavior in epithelial contact inhibition. *Proc. Natl Acad. Sci. USA* **109**, 739–744 (2012).
34. Brabletz, T., Kalluri, R., Nieto, M. A. & Weinberg, R. A. EMT in cancer. *Nat. Rev. Cancer* **18**, 128–134 (2018).
35. Haeger, A., Krause, M., Wolf, K. & Friedl, P. Cell jamming: collective invasion of mesenchymal tumor cells imposed by tissue confinement. *Biochim. Biophys. Acta* **1840**, 2386–2395 (2014).
36. Royou, A., Sullivan, W. & Karess, R. Cortical recruitment of nonmuscle myosin II in early syncytial *Drosophila* embryos: its role in nuclear axial expansion and its regulation by Cdc2 activity. *J. Cell Biol.* **158**, 127–137 (2002).
37. Martin, A. C., Gelbart, M., Fernandez-Gonzalez, R., Kaschube, M. & Wieschaus, E. F. Integration of contractile forces during tissue invagination. *J. Cell Biol.* **188**, 735–749 (2010).
38. Park, J. A., Fredberg, J. J. & Drazen, J. M. Putting the squeeze on airway epithelia. *Physiology (Bethesda)* **30**, 293–303 (2015).
39. Tschumperlin, D. J. et al. Mechanotransduction through growth-factor shedding into the extracellular space. *Nature* **429**, 83–86 (2004).
40. Trepat, X. et al. Physical forces during collective cell migration. *Nat. Phys.* **5**, 426–430 (2009).
41. Henkes, S., Fily, Y. & Marchetti, M. Active jamming: Self-propelled soft particles at high density. *Phys. Rev. E* **84**, 040301(R) (2011).
42. Angelini, T. E. et al. Glass-like dynamics of collective cell migration. *Proc. Natl Acad. Sci. USA* **108**, 4714–4719 (2011).
43. Nnetu, K. D., Knorr, M., Kas, J. & Zink, M. The impact of jamming on boundaries of collectively moving weak-interacting cells. *New J. Phys.* **14**, 115012 (2012).
44. Tambe, D. T. et al. Collective cell guidance by cooperative intercellular forces. *Nat. Mater.* **10**, 469–475 (2011).
45. Banigan, E. J., Illich, M. K., Stace-Naughton, D. J. & Egolf, D. A. The chaotic dynamics of jamming. *Nat. Phys.* **9**, 288–292 (2013).
46. Garrahan, J. P. Dynamic heterogeneity comes to life. *Proc. Natl Acad. Sci. USA* **108**, 4701–4702 (2011).

Acknowledgements

The authors thank M. L. Manning, H. Feldman and E. Millet for helpful discussions. This work was conducted with support from the Harvard Catalyst Clinical and Translational Science Center (National Center for Advancing Translational Sciences, National Institutes of Health Award UL1 TR001102) and financial contributions from Harvard University and its affiliated academic healthcare centres; the content is solely the responsibility of the authors and does not necessarily represent the official views of Harvard Catalyst, Harvard University and its affiliated academic healthcare centres, or the National Institutes of Health. This work was funded by the National Cancer Institute (grant number 1U01CA202123), the National Heart Lung and Blood Institute (grant numbers R01HL107561, PO1HL120839 and T32 HL007118) and the National Research Foundation of Korea (grant number NRF-2014R1A6A3A04059713).

Author contributions

L.A. designed and performed the HBEC experiment, developed the cell shape algorithm, analysed the corresponding data, contributed to manuscript preparation and oversaw the project. D.B. performed theoretical and computational analysis of the SPV model, guided analysis and interpretation of data and contributed to manuscript preparation. Y.S. analysed *Drosophila* data, assisted with statistical analysis and contributed to manuscript preparation. J.A.M. designed and performed layer maturation and compression experiments with HBECs and contributed to manuscript preparation. B.G. designed and performed stretching experiments with MDCKs. S.K. analysed MDCK data and performed computational simulations. S.J.D. designed the jamming superfamily figure and assisted with statistical analysis. B.L. assisted with preparation of slides in the HBEC experiment. J.H.K. analysed the dynamics of cellular motions in HBECs. R.H. assisted with cell culture in the HBEC experiment. A.F.P. designed and performed the experiments on MDCKs and contributed to manuscript preparation. K.H.L. performed statistical analysis. J.R.S. designed and performed statistical analysis. D.A.W. guided interpretation of the cell shape data. A.C.M. provided imaging data from *Drosophila* and contributed to manuscript preparation. J.-A.P. designed and guided the experiment on HBECs and contributed to the manuscript preparation. J.P.B. guided data interpretation and analysis, and contributed to manuscript preparation. J.J.F. oversaw the project, and contributed to experimental design, data analysis and manuscript preparation.

Competing interests

The authors declare no competing interests.

Additional information

Supplementary information is available for this paper at https://doi.org/10.1038/s41567-018-0089-9.

Reprints and permissions information is available at www.nature.com/reprints.

Correspondence and requests for materials should be addressed to J.J.F.

Publisher's note: Springer Nature remains neutral with regard to jurisdictional claims in published maps and institutional affiliations.

Methods

Culture of primary HBECs in ALI culture. Primary human bronchial epithelial cells (HBECs) were obtained at passage 0 or passage 1 from the Marsico Lung Institute/Cystic Fibrosis Center at the University of North Carolina, Chapel Hill. HBECs were cultured from three non-asthmatic and three asthmatic donors as previously described[4]. Briefly, passage 2 HBECs were seeded onto a Transwell insert coated with type I collagen (two Transwell inserts per donor), and grown under submerged conditions for five to six days until the cells reached confluence. On reaching confluence, medium was removed from the apical side of the Transwell insert, but was kept in the basal side to initiate air–liquid interface (ALI) culture conditions. Cells were maintained in ALI conditions and became well differentiated, expressing basal, goblet and ciliated cells (Supplementary Fig. 8), as seen in airways in vivo. On specific days of ALI culture, cells were fixed with 4% paraformaldehyde and stained with phalloidin conjugated with Alexa-488 to visualize F-actin (Life Technologies). Wide-field fluorescent images (10–20 per Transwell insert) were acquired at the apical plane on a Leica DMI 8 microscope using either a ×40 or ×63 oil objective (Leica), and automatically segmented and analysed using an in-house custom algorithm.

Cell morphology and metrics. Cell numbers progressively increased and projected areas progressively decreased with layer maturation (Fig. 1a and Supplementary Fig. 2a,d). Both in ALI culture and in vivo, the mature HBEC layer comprises mainly basal cells, goblet cells and ciliated cells arrayed in a complex pseudostratified structure (Supplementary Fig. 8). Cell shapes vary dramatically along the apical–basal axis, with the cell body often bulging in the vicinity of the nucleus, which is relatively stiff. Analysis of such systems typically emphasizes the dominant mechanical effects attributable to apical regions and the apical actin ring[5]. Fluorescent images labelled for F-actin show how these apical rings tile the cell layer (Fig. 1a and Supplementary Figs. 9–11). These rings were segmented using a customized algorithm (Supplementary Section 4), and from these segmented images we measured corresponding geometries across all donors and days of maturation in a total of 1.4×10^5 cells. For each ring, we determined the projected area and the aspect ratio, AR (Supplementary Fig. 11); the more slender or elongated the profile, the higher is its AR. For any closed ring in the cell plane, AR thus serves as a simple, primitive and robust metric of ring shape. In a previous study, we had used as an index of shape the factor q, which is the ring perimeter divided by the square root of area[4]. Although AR and q were correlated in the data set described here, we found that the experimentally observed range of AR spanned roughly fivefold whereas that of q spanned less than twofold (Supplementary Fig. 7). To better resolve changes in shapes, we found it preferable to use AR.

Migratory dynamics. Collective migratory dynamics in this experimental system have been characterized previously[4], and we use a variety of metrics here to replicate and confirm those earlier findings (Supplementary Fig. 1). For example, within the confluent layer, cells move in cooperative swirls or packs of 10–100 cells. These packs display characteristic pack speed, size and lifetime (as determined from the peak of the four-point susceptibility), and after several pack lifetimes any individual cell finds itself surrounded by a different set of immediate neighbours. As the jamming transition is approached, pack speed tends to decrease as pack size and pack lifetime tend to grow[4], but there is no objective cutoff that defines a jamming transition. Rather, the transition is gradual and continuous, and jamming is said to occur when pack lifetime grows to exceed the laboratory measurement window (144 min). Using those criteria, the non-asthmatic maturing HBEC layer approaches jamming by day 8 of ALI culture, whereas the asthmatic layer approaches jamming no sooner than day 14[4].

MDCK culture and live imaging. Cells were stably transfected with green fluorescent protein (GFP)-linked nuclear localization signal and cultured in Dulbecco's modified Eagle's medium supplemented with 10% fetal bovine serum, 1% penicillin/streptomycin and 0.5 mg ml^{-1} G418. Tissue culture plates were coated with collagen I and 50,000 cells were added to the centre of the well and allowed to adhere for 24 h. Cells were maintained at 37 °C and 5% CO_2 as images were recorded every 3 min for 54 h using phase microscopy and confocal fluorescence using the 488 nm line of an argon laser on a Leica DMI6000 SP5 microscope with a stage top incubator. Images were processed to find the centroid of each nucleus, and the locations of the centroids were used as seeds for a Voronoi tessellation to create a polygonal tiling of the cell layer. These polygons were then used to obtain cell AR using an in-house custom algorithm.

Fly stocks and live imaging. The following fly lines were used for imaging: *sqh*::*GFP* (myosin regulatory light chain, *sqh*, fused to GFP and expressed from the endogenous promoter)[47], *Gap43–mCherry* (membrane marker driven by the *sqh* promoter)[48]. To make maternal-effect concertina (*cta*) mutant embryos, the *cta*^{RC10}; *sqh*::*GFP, Gap43*::*mCherry/TM3* flies were crossed with *Df(2 L)PR31/CyO, sqh*::*GFP* flies and embryos from non-balancer F1 females were imaged.

For live-cell imaging of *Drosophila*, embryos were dechorionated with 50% commercial bleach, washed with water, and mounted ventral side up on a glue-coated microscope slide. Two No. 1.5 coverslips were put between the slide and the top coverslip to make a chamber and avoid compressing the embryo. Embryos were imaged in halocarbon 27 oil (Sigma-Aldrich). Images were acquired using a Zeiss LSM 710 confocal microscope equipped with a x ×40/1.2 numerical aperture Apochromat water objective (Carl Zeiss). For each time point, z projections of three consecutive slices were automatically segmented and analysed using an in-house custom algorithm.

RNAi knockdown in *Drosophila*. To disrupt the Twist transcription factor, the embryo is injected with double-stranded RNA (dsRNA) generated using the Invitrogen MEGAscript T7 transcription kit, resuspended in 0.1 × PBS[17]. The dsRNA against Twist had to be injected at least 2.5 h before imaging/gastrulation in order to observe the phenotype. The following primers were used to generate Twist dsRNA: forward: 5′-TAATACGACT CACTATAGGGGCCAAGCAAGATCACCAAAT-3′; reverse: 5'-TAATAC GACTCACTATAGGGGACCTCGTTGCTGGGTATGT-3'.

Maximum-likelihood estimation. We fitted the k-gamma probability density, $\mathrm{PDF}(x;k)=k^k x^{k-1}\mathrm{e}^{-kx}/\Gamma(k)$, to the data by the method of maximum likelihood. For each data set, ARs were shifted and normalized by $x=(\mathrm{AR}-1)/(\overline{\mathrm{AR}}-1)$. For a given set of data $\{x_i\}\, i=1,\ldots,N$, the likelihood function is

$$L(k)=\prod_{i=1}^{N}\rho(x_i;k)$$

The maximum-likelihood estimate of k is then given by $\hat{k}=\mathrm{argmin}\,|_k(-\ln L(k))$. The CIs for $\hat{k}$ were determined by parametric bootstrapping as follows. N simulated data points were generated from the cumulative distribution function corresponding to the $\hat{k}$ for that set. Maximum likelihood was again performed, yielding a parameter estimate $\hat{k}_1$ from this first set of simulated data. This procedure was repeated over a large number S of simulations, typically > 200. The standard deviation of the resulting set $\{\hat{k}_s\}, s=1,\ldots,S$ was used to construct 95% CIs.

Finally, we tested goodness-of-fit for this approach by computing chi squared values. For each data set, we constructed (uniform) decile bins from the cumulative distribution function, given $\hat{k}$ for that set. We counted the observed number of data points $O_j, j=1,\ldots,10$ occurring within each bin, and compared these with the expected number of occurrences $E=N/10$ within each bin by computing,

$$\chi^2=\sum_{j=1}^{N}(O_j-E)^2/E$$

For decile binning, the number of degrees of freedom is 9; the threshold value of χ^2 for 95% confidence is given by $\chi^2_{0.05,9}=16.9$. Observed values of $\chi^2>\chi^2_{0.05,9}$ indicate a rejection of goodness-of-fit with 95% confidence.

For HBEC data, we found that out of 646 frames, only 22 had $\chi^2>\chi^2_{0.05,9}$, or approximately 3.4%. This is close to the expected false negative rate of 5%, given an appropriate distribution function with 95% confidence limits. Similarly, the data from *Drosophila* revealed a fraction of $\chi^2>\chi^2_{0.05,9}$ also approximately 3.4%, and the MDCK data exhibited a fraction of 9.8%. This is striking confirmation at the level of goodness-of-fit that the underlying distribution over these cell types is well characterized by the k-gamma distribution given in equation (1).

Data availability. Data that support the plots within this paper and other findings of this study are available from the corresponding author upon request.

References

47. Schall, P., Weitz, D. A. & Spaepen, F. Structural rearrangements that govern flow in colloidal glasses. *Science* **318**, 1895–1899 (2007).
48. Mattsson, J. et al. Soft colloids make strong glasses. *Nature* **462**, 83–86 (2009).